Physica C 469 (2009) 55–59

Contents lists available at ScienceDirect

Physica C

journal homepage: www.elsevier.com/locate/physc

Increase of critical current density with doping carbon nano-tubes in $YBa_2Cu_3O_{7-\delta}$

S. Dadras [a], Y. Liu [b], Y.S. Chai [b], V. Daadmehr [a], K.H. Kim [b,*]

[a] Magnetic and Superconducting Res. Lab., Department of Physics, Alzahra University, P.C.1993891176 Tehran, Iran
[b] eXtreme Multifunctional Physics Laboratory, FPRD, School of Physics and Astronomy, Seoul National University, Seoul 151-747, Republic of Korea

ARTICLE INFO

Article history:
Received 27 October 2008
Accepted 11 November 2008
Available online 25 November 2008

PACS:
74.25.Sv
74.72.Bk
74.62.Dh
61.48.De

Keywords:
Critical current density
$YBa_2Cu_3O_{7-\delta}$
Carbon nano-tube doping

ABSTRACT

The effects of carbon nano-tubes (CNTs) on the crystal structure and superconducting properties of $YBa_2Cu_3O_{7-\delta}$ (Y-123) compound were studied. Samples were synthesized using standard solid-state reaction technique by adding CNT up to 1 wt% and X-ray diffraction data confirm the single phase orthorhombic structure for all the samples. Current–voltage measurements in magnetic fields up to 9 T were used to study the pinning energy U_J and critical current density J_c as a function of magnetic field at fixed temperature. We find that while T_c does not change much with the CNT doping (91–92 K), both U_J and J_c increase systematically up to 0.7 wt% CNT doping in a broad magnetic field ranges between 0.1 and 9 T and J_c in the 0.7 wt% CNT doped sample is at least 10 times larger than that of the pure Y-123. The scanning electron microscope image shows that CNTs are forming an electrical-network between grains. These observations suggest that the CNT addition to the Y-123-compounds improve the electrical connection between superconducting grains to result in the J_c increase.

1. Introduction

Since the discovery of high temperature superconductivity (HTSC), various attempts have been carried out to enhance the critical current density J_c and to optimize critical temperature T_c in these materials. In recent years, various kinds of doping, including metal and nonmetal elements, various carbon sources, nano-particles, carbon nano-tubes and other compounds have been used to improve both the inter- and intragranular J_c in different high temperature superconductors. In addition, superconducting properties have shown dependence on chemical compound and impurities. The type and amount of dopants and preparation methods in high temperature superconductors have had important influences on the structure and the dopant substitution site [1].

$YBa_2Cu_3O_{7-\delta}$ (Y-123) superconductor can be effective for practical applications due to its high T_c. However, the flux pinning of the Y-123 is weak so that J_c is relatively small, especially at temperatures above 20–30 K [2]. By pinning the flux lines effectively, we can prevent the vortex movements and increase the critical current density. Therefore, it will be necessary to prepare samples with more artificial pinning centers to increase the critical current density.

Nano-phase particles in the superconductor matrix can increase the intragranular critical current density under high magnetic fields [3]. Among various carbon precursors, carbon nano-tubes (CNTs) are particularly interesting due to their nanometer diameter that can serve as the effective pinning centers, compared to the ordinary carbon [4,5]. The magneto-optical investigations indeed show that nano-tubes are functioning like-columnar defects produced by heavy-ion irradiation, which increases the transport current density [5]. The carbon nano-tubes with diameters almost coinciding with the coherence length ξ in the *ab*-plane are expected to act as efficient pinning centers in HTSC materials [6,7]. Therefore, doping effects of single-walled and multi-walled carbon nano-tubes on T_c, lattice parameters, J_c(B), microstructure and H_{C2} of MgB_2 superconductors have been studied [8–11]. Generally, T_c decreased and J_c increased with the CNT increase in these compounds. In addition to the intragranular effects, the enrichment of the inter-granular electrical links could have effective role in the increase of J_c, since the existence of electrically coupled grains or clusters can make inter-granular current flow increase.

Up to now, the effects of CNT doping on the Y-123 compound have not been reported yet. With the typical length of the CNT (>∼1 μm) larger than the coherence length (∼2 nm) of the Y-123 compound in general, the CNTs doping in the Y-123 compound is expected to increase the J_c via the amplification of the electrical links, not via the intragranular effects. With this motivation, we investigate the microstructure and critical current density of the bulk Y-123 samples with different CNT doping and discuss the role of CNTs as a possible source of additional electrical links. The analyses of the current (*I*)–voltage (*V*) chracteristics using the Zeldov

* Corresponding author. Tel.: +82 2 880 9068; fax: +82 2 888 0769.
E-mail address: khkim@phya.snu.ac.kr (K.H. Kim).

0921-4534/$ - see front matter © 2008 Elsevier B.V. All rights reserved.
doi:10.1016/j.physc.2008.11.004

model for pinning energy [12,13], explain the magnetic field- and CNT doping-dependences of critical current density J_c and pinning energy U_J. We find the increases of U_J and J_c with increase of the CNT doping up to 0.7 wt% in different magnetic fields up to 9 T.

2. Experimental

2.1. Catalytic synthesis of carbon nano-tubes

We used chemical vapor deposition (CVD) method for carbon nano-tubes synthesis. Carbon nano-tubes and nano-fibers are graphitic filaments with diameters ranging from 0.4 to 500 nm and lengths in the range of several micrometers to millimeters. The growth of CNTs involves the catalytic decomposition of hydrocarbons on metal catalysts (typically Fe, Ni, Co), carbon diffusion on it and its precipitation as a filament [14]. We use high purity Ar (99.999%) as a carrier gas and acetylene as a feed stock in the rate of 4 to 1. We used a wet catalyst method, in which a liquid solution containing the catalyst in a salt form [$(Co(NO_3)_2 \cdot 6H_2O)$ and/or $(Ni(NO_3)_2 \cdot 6H_2O)$] is applied to the substrate via spin coating. After application to the substrate, the salt solution is often reduced to oxide nano-particles by calcinations (i.e., heating in air) [15]. The metal oxides are stable and improve the catalyst-support interaction at the growth temperature [16]. During the growth, these oxides are reduced to metal nano-particles (e.g. using hydrogen) which catalyze the subsequent growth of carbon nano-tubes or nano-fibers.

2.2. Samples preparation

The samples were prepared by the conventional solid-state reaction method. High purity powders of Y_2O_3, $BaCO_3$ and CuO (99.99%) with the exact stochiometry were mixed. After grinding and calcinations at 812 °C in air, we mixed the Y-123 powder with different percentage of CNTs weight (0.3–1 wt%). For obtaining more homogenous mixing, we suspended it in an organic solvent with an ultrasonic mixer to prevent agglomeration of CNTs. The CNT-Y-123 powder was dried afterwards, and pressed as pellets at 1000 MPa in the form of circular disks of about 1 mm thick and 10 mm diameter. The pellets were sintered at 930 °C in oxygen atmosphere. Since the samples are in the tetragonal phase at 930 °C, we cooled down the sample in a flowing oxygen condition and make it well oxygenated. Then, the sample became a predominately orthorhombic phase from the tetragonal to orthorhombic structural phase transition at 630 °C [17]. The samples were cut into a rectangular strip and the electrical leads were attached by using silver paste. The critical temperature and resistivity of the prepared sample with different doping weights of CNT are measured with the standard four-probe-method.

We investigated the structure and phase of the samples by powder X-ray diffraction (XRD) using a Philips diffractometer with Cu K_α radiation. The diffraction data were collected over the diffraction angle range of $2\theta = 20$–$70°$ by a step scan with a width of 0.02°. The microstructure and phase composition of the samples were investigated using scanning electron microscopy (SEM) (Philips, XL30 model) equipped with energy dispersive analysis of X-ray. The electrical resistivity was measured with using a model SR830 lock-in amplifier with a constant current of 0.5 mA and 17 Hz frequency from 50 to 100 K.

3. Results and discussion

3.1. Structural and superconducting properties

The single orthorhombic phase of Y-123 is confirmed by XRD, as shown in Fig. 1, for various CNT doping levels from 0.0 to 1.0 wt% CNT. The XRD patterns were analyzed by the Rietveld structure refinement method. The diffraction peaks have been indexed with the orthorhombic indices. The presence of (030), (001), (120), (021), (130), (031), (050), (131), (060), (200), (002), (161), (132), and (202) peaks in the XRD patterns confirms the formation of a Y-123 single phase. The lattice parameters are calculated to be $a = 3.8202$ Å, $b = 3.8854$ Å and $c = 11.6834$ Å for the all samples.

The temperature-dependent resistivity for pure and CNT doped samples is shown in Fig. 2. All samples show metallic behavior in the normal state and a superconducting transition to zero resistance, with good critical transition temperature between 92 and 94 K. Also, the transition width ΔT_c is nearly constant (3–3.5 K) and shows sharp transition for all samples, which indicates that the preparation and synthesis of samples procedure are done correctly. The temperatures for the onset of the resistivity drop T_c^{on}, for the middle point T_c^{mid}, and for the zero resistance $T_c(0)$ versus the CNT doping are summarized in Fig. 3. Although T_c of the 0.3 wt% doping is slightly larger, all the CNT doped Y-123 show more or less similar transition temperatures between 91 and 92 K as determined from T_c^{mid}.

In order to investigate the broadening of the resistive transition in the CNT doped Y-123 compound, we measured the resistivity under magnetic field up to 9 T, applied perpendicular to the current and the flat surface of the samples. Fig. 2 shows the magneto-resistance data measured as a function of the temperature for a fixed current of $I = 0.5$ mA. These curves show two distinct features; a steep decrease associated with the onset of the superconductivity of the individual grains, and a longer transition tail due to the weak link coupling between the grains. As the applied magnetic field is increased, for all the samples, the normal-state

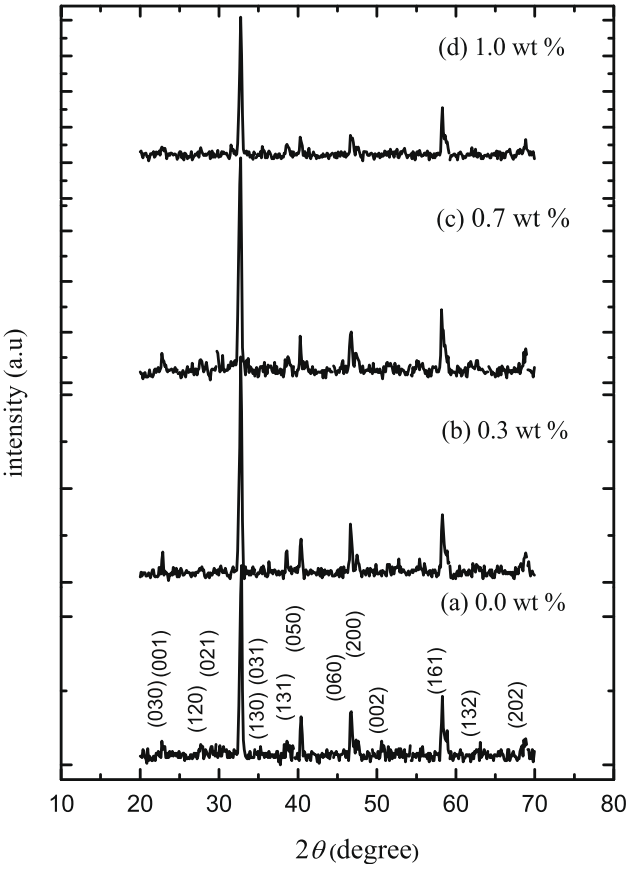

Fig. 1. XRD patterns of Y-123 samples with (a) 0.0, (b) 0.3, (c) 0.7, and (d) 1.0 wt% CNT doping.

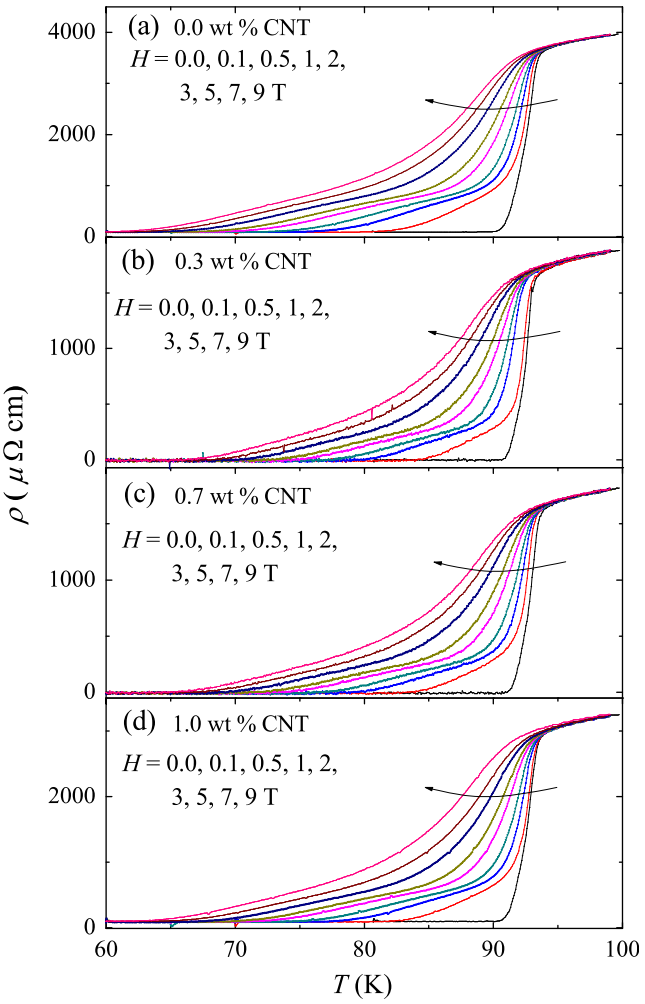

Fig. 2. Resistivity versus temperature for (a) pure and (b) 0.3 (c) 0.7 and (d) 1.0 wt% CNT doped Y-123 sample in different magnetic fields up to 9 T.

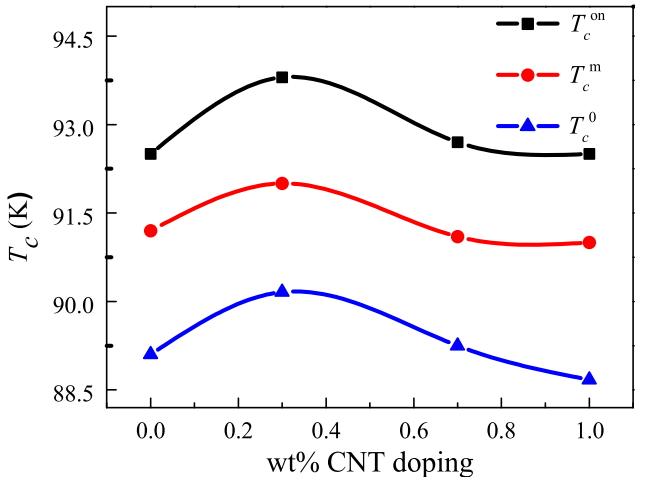

Fig. 3. Critical temperature T_c^{on}, T_c^{mid} and T_c^{0} vs. CNT doping (wt%).

resistivity does not show appreciable change; while for each sample, $T_c(H)$ moves to considerably lower temperatures. Thus, the resistive transition is broadened as the magnetic field is increased [18]. At low temperatures, close to $T_c(H)$, a long range superconducting state with zero resistance is achieved by means of a percolation-like process that controls the activation of weak links between grains. Under applied magnetic field, the weak links are affected and therefore, the tail part dissipates even in small fields. In large magnetic fields, due to flux penetration inside the grains, the onset part of transition will be broadened [19].

We note in Fig. 2 that the resistivity for the CNT doped samples is less than the pure sample resistivity in general. For example, the resistivity of the pure sample at 100 K is about two times larger than those of the samples with the 0.3 and 0.7 wt% CNTs and it is still slightly larger than that of the sample with the 1 wt% CNT doping. Therefore, CNT doping overall results in decrease of resistivity values in this compound. Moreover, we note that the tail part of the resistivity measured at H = 9 T in the pure sample (Fig. 2a) is longer than the doped ones (Fig. 2b and c), and continue down to 60 K. This observation suggests that the addition of the CNT has reduced the number of effective weak links across the grain boundary in the pure sample. On the other hand, the resistivity of the 1 wt% CNT doping does not show further increase of the tail parts. Therefore, these observations already suggest that the 0.7 wt% CNT doping can be optimal for the reduction of the weak links and that the systematic study of J_c is needed through the current (I)–voltage (V) analyses for these series of samples.

3.2. Current–voltage characteristics

The I–V characteristics of the superconducting samples can gives us further insight into the character of the inter-grain links and into the vortex pining centers. For bulk HTSCs with poor grain alignment and texture, I–V characteristics are governed by the weak links between the grains, because the intra-grain J_c is much higher than the inter-grain J_c. The links between the grains will form randomly distributed Josephson junctions, each of which has a different value of the local critical current density. In particular, the transport in the present Y-123 pellets is likely to be controlled by the grain boundaries, since in superconducting state the electrical resistivity of each grain is negligible. The critical current can decrease very abruptly with the magnetic field if the weak superconducting links exist across the grain boundaries. Only the current through the boundaries that were not weak links can remain at elevated fields.

With regard to the models for the J-dependence of U_J, a linear relation has been presented by Anderson and Kim (AK) for low temperature superconductors [20]. An inverse power law barrier has also been proposed by Feigelman et al. [21] and a logarithmic barrier has been proposed by Zeldov et al. for HTSCs [12]. Our data are indeed consistent with Ref. [12] that suggests a logarithmic potential barrier for the flux pinning, i.e.,

$$U_{\mathrm{eff}}(T,H,J) = U_J(T,H)\ln(J_c/J), \tag{1}$$

where U_J is the characteristic pinning potential energy in the fixed current density [22]. We substituted U_{eff} from the model in Ref. [12] into

$$E = E_0 \exp(-U_{\mathrm{eff}}/k_B T). \tag{2}$$

Taking the logarithm of this relation gives

$$\ln(E) = [\ln(E_0) - U_J/k_B T \ln(JC)] + U_J/k_B T \ln(J). \tag{3}$$

Thus, one can calculate U_J from the slope of the $\ln E$ vs $\ln J$ curves.

Fig. 4 shows E–J curves of (a) pure, (b) 0.3, (c) 0.7, and 1.0 wt% CNT doped Y-123 samples, respectively, at different magnetic fields up to 9 T and at 70 K. From the slope of the linear part in the high J-regime [12], we obtained U_J according to the Eq. (3). Furthermore, to estimate J_c variation with temperature and magnetic field, we defined J_c as the current density at the lowest E measured throughout all of the samples, i.e., 1 V/m in this case. Thus determined J_c and U_J are summarized in Figs. 5 and 6, respectively,

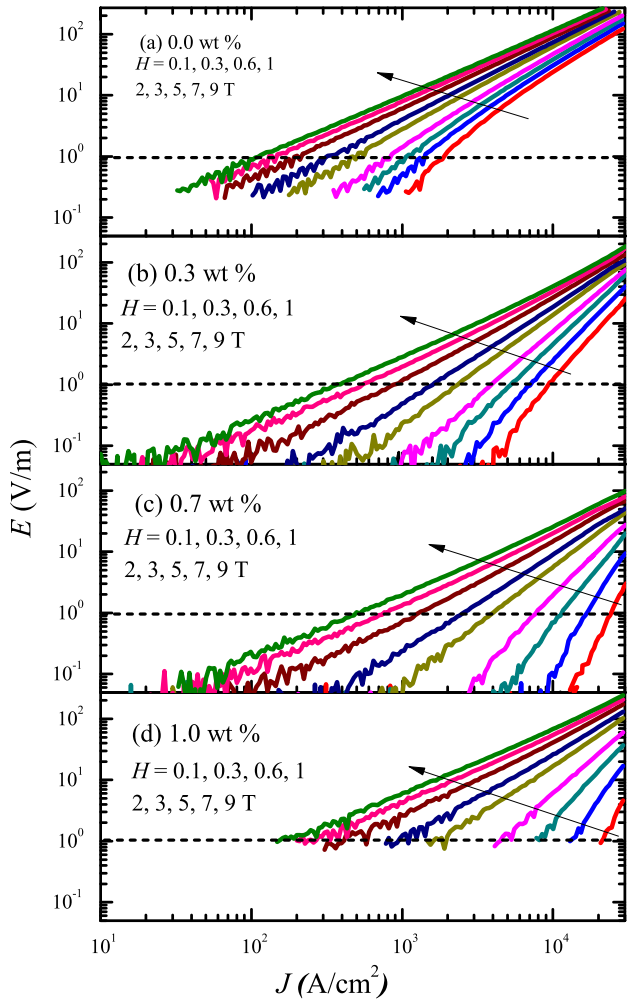

Fig. 4. *E–J* curves of pure and CNT doped Y-123 samples with different amount, (a) 0.0 (b) 0.3 (c) 0.7, and (d) 1.0 wt% at 70 K and at magnetic field *H* between 0.1 and 9 T.

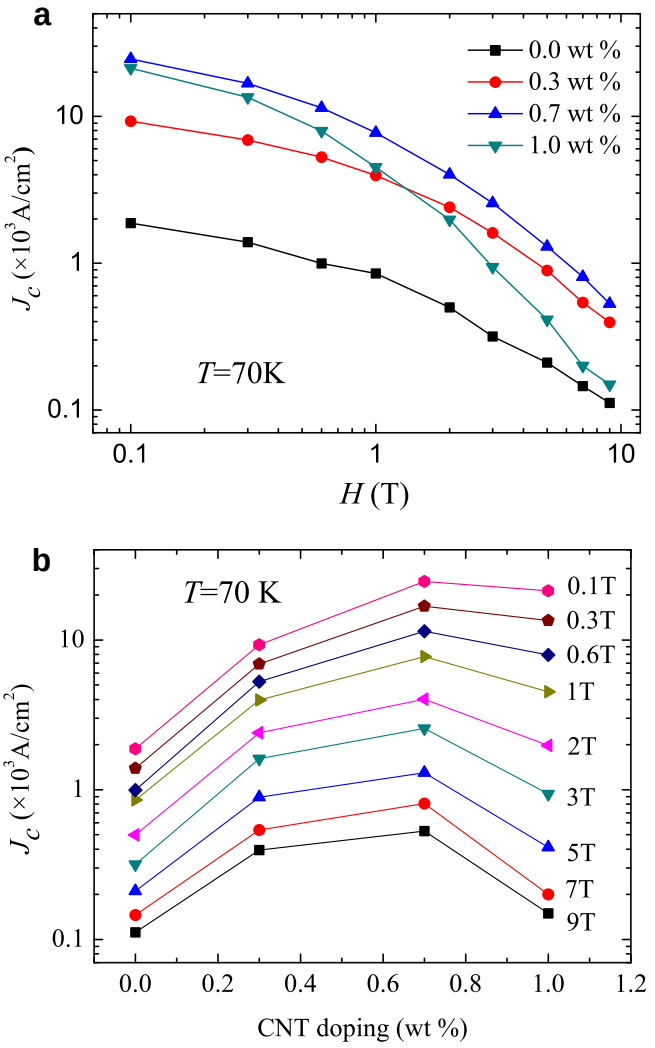

Fig. 5. (a) J_c vs. H for different CNT doping and (b) J_c vs. percentage of the CNT doping.

showing the changes of J_c with the CNT doping in different magnetic field. As shown in Fig. 5a, with the increase of the CNT doping, J_c increases significantly. At $H = 0.1$ T, the sample with 0.7 wt% CNT doping has 10 times larger J_c than the pure one. We also note that the J_c increase in higher magnetic field (>1 T), with respect to the CNT doping, becomes smaller (5 times) than in lower magnetic field (<1 T). At $H = 9$ T, the sample with 0.7 wt% CNT doping has about five times larger J_c than the pure one. On further increasing the CNT doping up to 1.0 wt%, J_c remained almost same at low field below 0.6 T but decreased above. Thus, 0.7 wt% CNT doping shows the optimum for the J_c increase. Consistent with this behavior, we also find in Fig. 6 that U_J systematically increase with the CNT doping up to 0.7 wt% and it becomes slightly lower for the 1 wt% CNT doping. The decrease of J_c and U_J in the 1.0 wt% CNT sample might be related to the increased disorder effect with the CNT doping as the resistivity of this sample has increased more than the 0.7% sample as discussed above.

To further understand the role of the CNT doping, the microstructure of the samples was investigated using the SEM as shown in Fig. 7. The SEM picture in Fig. 7a shows that the pure Y-123 has bad grain connections. When doped with the 0.3 wt% CNT, it seems that the grain connection becomes a little better (Fig. 7b). More close look with higher magnification in Fig. 7c and d reveals that the carbon nano-tubes exist in-between spaces of the grains and connect the grains electrically. Thus, it is likely that the CNT connections produce the electrical link between the grains to help the inter-granular current flow. Therefore, the increase of J_c as

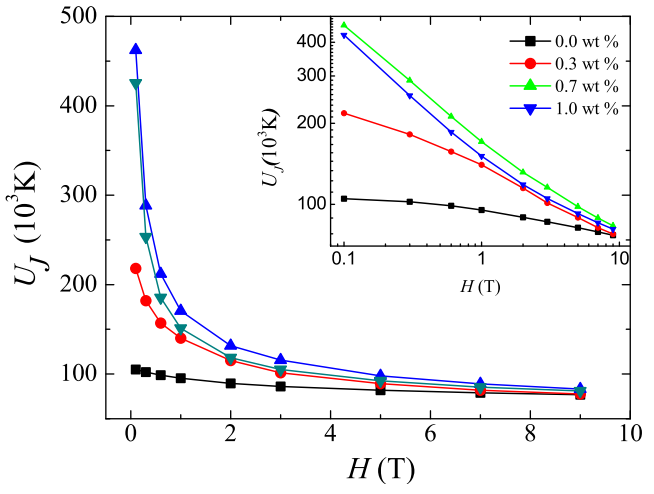

Fig. 6. Pinning energy vs. H for the CNT doped Y-123 samples. The inset shows U_J vs. H in a logarithmic scale.

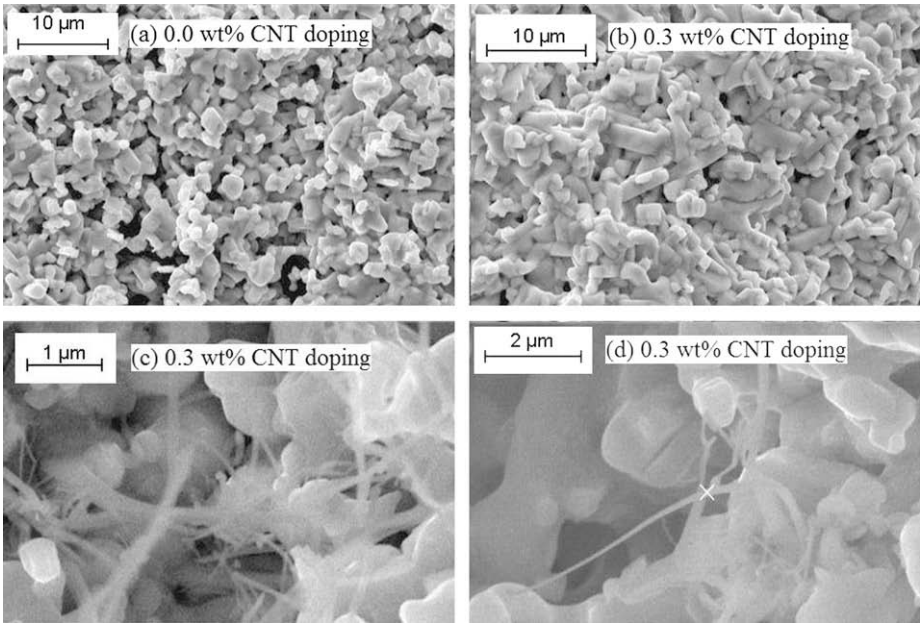

Fig. 7. SEM pictures of (a) pure, (b), (c) and (d) CNT doped samples. The (c) and (d) indicate that CNTs in the samples helps the electrical connectivity between grains.

observed in the 0.3 and 0.7 wt% CNT doped samples seems to be related to the enhanced inter-granular current flow.

On the other hand, as demonstrated in Figs. 5 and 6, not only J_c but also U_J increases with the CNT doping. This means that with the CNT doping, the vortex pinning increases. Although it is not clear from the SEM picture, this fact indicates that low doping level of CNTs might act as columnar defects that were proven to be very strong pinning centers in HTSC compounds [5]. We further note that the increase of J_c as well as U_J occurs more sensitively at a low magnetic field region in Figs. 5 and 6. For example, the increased U_J of the 0.7 wt% sample at $H = 0.1$ T is about four times than that of a pure sample while the increase reaches less than 10% at $H = 9$ T. Thus, in future possible applications, the addition of CNTs to Y-123 can be effective in enhancing the superconducting properties such as critical current density and pinning energy in a relatively low magnetic field region below 1 T.

4. Conclusions

We have investigated the CNT doping effects on the critical current density and vortex pinning energy in the $YBa_2Cu_3O_{7-\delta}$ polycrystlline specimens through the current–voltage characteristics. Both critical current density and the vortex pinning have increased up to the 0.7 wt% of the CNT doping and decreased on further increased doping amount. Our results suggest that the relatively low CNT doping can improve the electrical links between superconducting grains in $YBa_2Cu_3O_{7-\delta}$ to enhance the inter-granular current flow.

Acknowledgments

This work has been supported by NRL program (M10600000238) and GPP-KICOS program (K20702020014-07E0200-01410) by MEST, the fundamental R&D program for core technology of materials by MOKE, and in part by the office of Vice President for Research and Graduate Studies at Alzahra University. The authors would like to thank Professor M. Akhavan for fruitful discussions.

References

[1] A. Mellekh, M. Zouaoui, F.B. Azzouz, M. Annabi, M.B. Salem, Solid State Commun. 140 (2006) 318.
[2] M.R. KoblischKa, S.L. Huang, K. Fossheim, T.H. Johansen, H. Bratsberg, Physica C 300 (1998) 207.
[3] K.C. Goretta et al., United State Patent 5,929,001, July 1999.
[4] K. Fossheim, E.D. Tuset, T.W. Ebbesen, M.M.J. Treacy, J. Schwartz, Physica C 248 (1995) 195.
[5] S. Huang, M.R. Koblischka, K. Fossheim, T.W. Ebbesen, T.H. Johansen, Physica C 311 (1999) 172.
[6] T.W. Ebbesen, P.M. Ajayan, Nature 358 (1992) 220.
[7] T.W. Ebbesen, Annu. Rev. Mater. Sci. 24 (1994) 235.
[8] S.X. Dou, W.K. Yeoh, J. Horrat, M. Ionescu, Appl. Phys. Lett. 83 (2003) 4996.
[9] W.K. Yeoh, J. Horvat, S.X. Dou, V. Keast, Supercond. Sci. Technol. 17 (2004) 572.
[10] J.H. Kim, W.K. Yeoh, M.J. Qin, X. Xu, S.X. Dou, J. Appl. Phys. 100 (2006) 013908.
[11] J.H. Kim, W.K. Yeoh, M.J. Qin, X. Xu, S.X. Dou, P. Munroe, H. Kumakura, T. Nakane, C.H. Jiang, Appl. Phys. Lett. 89 (2006) 122520.
[12] E. Zeldov, N.M. Amer, G. Koren, A. Gupta, M.W. McElfresh, R.J. Gambino, Appl. Phys. Lett. 56 (1990) 680.
[13] L. Shan, A.M. Sun, X.N. Xu, Y.L. Tang, D.W. Lu, X. Jin, L.J. Shen, C.C. Lam, Y.S. Chen, Supercond. Sci. Technol. 12 (1999) 1138.
[14] H. Terrones, T. Hayashi, M. Munoz-Navin, M. Terrones, Y.A. Kin, N. Grobert, R. Kamalakaran, J. Dorants-Davila, R. Escudero, M.S. Dresselhouse, M. Endo, Chem. Phys. Lett. 343 (2001) 241.
[15] R.T.K. Baker, J.R. Alonzo, J.A. Dumesic, D.J.C. Yates, J. Catal. 77 (1982) 74.
[16] J. Kong, A.M. Cassell, H.J. Dai, Chem. Phys. Lett. 292 (1998) 567.
[17] S. Dadras, M. Hekmat, M.R. Safari, V. Daadmehr, Iran. J. Phys. Res. 6 (2006) 201.
[18] M. Akhavan, Physica B 321 (2002) 265.
[19] M.R. Mohammadizadeh, M. Akhavan, Physica C 390 (2003) 134.
[20] P.W. Anderson, Y.B. Kim, Rev. Mod. Phys. 36 (1964) 39.
[21] M.V. Feigelman, V.B. Geshkenbein, A.I. Larkin, V.M. Vinokur, Phys. Rev. Lett. 63 (1989) 2303.
[22] G. Blatter, M.V. Feligelman, V.B. Geshkenbein, A.I. Larkin, V.M. Vinokur, Rev. Mod. Phys. 66 (1994) 1125.